Journal of Hydrology 662 (2025) 134001

Contents lists available at ScienceDirect

Journal of Hydrology

journal homepage: www.elsevier.com/locate/jhydrol

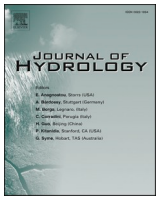

Research papers

Greenland supraglacial lakes albedo-depth parameterization from multi-source remote sensing: An application of lake-albedo feedback modeling

Jiake Wu [a,b], Lei Zheng [a,b,*], Zhuoqi Chen [a,b], Quan Zhou [a,b], Chuyue Peng [a,b], Qi Liang [a,b], Teng Li [a,b], Baojuan Huai [c], Weijun Sun [c], Xiao Cheng [a,b], Robert Law [d,e], Fengming Hui [a,b,*]

[a] School of Geospatial Engineering and Science, Sun Yat-sen University & Southern Marine Science and Engineering Guangdong Laboratory (Zhuhai), Zhuhai 519082, China
[b] Key Laboratory of Comprehensive Observation of Polar Environment (Sun Yat-sen University), Ministry of Education, Zhuhai 519082, China
[c] College of Geography and Environment, Shandong Normal University, Jinan 250014, China
[d] Department of Earth Science, University of Bergen, Bergen 5007, Norway
[e] Bjerknes Centre for Climate Research, Bergen 5007, Norway

ARTICLE INFO

This manuscript was handled by Yuefei Huang, Editor-in-Chief, with the assistance of Baoqing Zhang, Associate Editor

Keywords:
Greenland Ice Sheet
Supraglacial lakes
Remote sensing
Albedo parameterization
Lake albedo feedback

ABSTRACT

Supraglacial lakes (SGLs) diminish surface albedo, thereby amplifying solar radiation absorption and accelerating ice sheet mass loss. This constitutes a critical but poorly quantified feedback, primarily due to the limited observational capacity and an incomplete understanding of the bottom ablation processes within SGLs. In this study, we improved the SGL model GlacierLake_v2 by incorporating a specific albedo-depth parameterization developed from Sentinel-2 and ICESat-2 observations and a meteorologically driven runoff module to account for meltwater input. Validating against in-situ observation suggests the GlacierLake_v2 shows promising performance in SGL bottom ablation estimation, with a root mean square error (*RMSE*) of 1.2 cm. Our simulations reveal that the SGL-albedo feedback has increased the summer ice melt rate by 122 % in Lake BlueSnow, and the feedback decreases exponentially with lake depth. Additionally, the presence of SGLs mitigates the temporary reduction in ice melt rates typically induced by summer snowfall. These findings highlight the importance of incorporating SGL-albedo feedback in the Greenland ice sheet hydrological and mass balance modeling in a warming Arctic.

1. Introduction

There has been pronounced warming of the Greenland ice sheet (GrIS) since the 1990s (Hanna et al., 2021; Zhang et al., 2022), and increased surface meltwater runoff has been shown to dominate the recent mass loss of the GrIS (van den Broeke et al., 2017). Meltwater accumulates in depressions, forming supraglacial lakes (SGLs), which play a critical role in ice sheet dynamics. As an important buffer carrier, SGLs delay the entry of meltwater into the ocean (Ran et al., 2024). However, meltwater from SGLs rapidly penetrates to the ice sheet base through hydraulic fracturing or moulins, enhancing basal lubrication and affecting seasonal ice flow (Chudley et al., 2019; Johansson et al., 2013; Maier et al., 2023). Compared to surrounding snow and ice, lower albedo makes SGLs absorb more solar radiation and accelerates ablation at the lake bottom (Lüthje et al., 2006; Tedesco et al., 2012). This positive feedback mechanism substantially contributes to the GrIS's overall mass loss. To better understand the role of SGL-albedo feedback in modulating mass balance, it is essential to estimate the SGL bottom ablation rate.

In-situ measurements of SGLs are sparse, limited by extreme weather conditions and hazardous working environments. The bathymetry data, the primary variable measured during the field survey, were usually obtained using a sonar transducer installed on a remote-controlled boat (Box and Ski, 2007; Fitzpatrick et al., 2014; Legleiter et al., 2014; Lutz

* Corresponding authors at: School of Geospatial Engineering and Science, Sun Yat-sen University & Southern Marine Science and Engineering Guangdong Laboratory (Zhuhai), Zhuhai 519082, China.
E-mail addresses: zhenglei6@mail.sysu.edu.cn (L. Zheng), huifm@mail.sysu.edu.cn (F. Hui).

https://doi.org/10.1016/j.jhydrol.2025.134001
Received 4 March 2025; Received in revised form 21 July 2025; Accepted 29 July 2025
Available online 30 July 2025

et al., 2024; Tedesco and Steiner, 2011). Multi-spectral reflectance with wavelengths ranging from 450–605 nm and 350–1025 nm was recorded in Lake Olivia (Tedesco and Steiner, 2011) and Lake Napoli (Legleiter et al., 2014), respectively. In addition, observed lake temperature and bottom ablation rates in western GrIS were first reported by Tedesco et al. (2012). While these studies have provided valuable insights, they remain limited in number and coverage.

The accessibility and broad coverage of remote sensing have driven significant advances in SGLs over the past decade. SGLs can be extracted from optical images and SAR data (Asadi et al., 2025; Jiang et al., 2022; Lu et al., 2021; Yang and Smith, 2013; Zheng et al., 2023). Lake depth can be derived from optical images using the physically radiative transfer equation and empirical method (Pope et al., 2016), but the physically based method tends to underestimate and overestimate when using red and green bands, respectively (Melling et al., 2024). In addition, the depression topography method can be used to estimate lake depth by differencing DEMs acquired before and after the drainage of an SGL (Lutz et al., 2024; Melling et al., 2024; Yang et al., 2019; Zhou et al., 2025), particularly when in-situ measurements are unavailable (Man et al., 2025). The Ice, Cloud, and Land Elevation Satellite-2 (ICESat-2) has recently provided new potential for derived SGLs depth (Arndt and Fricker, 2024; Fricker et al., 2021; Xiao et al., 2023; Datta and Wouters, 2021). Lutz et al. (2024) established an empirical relationship between single-band Sentinel-2 reflectance and ICESat-2-derived SGLs depth, and applied it to estimate the depth and volume of four SGLs in the northeastern GrIS. Machine learning has also been applied to water-related retrieval tasks (Ahmadianfar et al., 2022; Iman Ahmadianfar et al., 2023; Kordani et al., 2024; Samadi-koucheksaraee et al., 2019; Samadi-Koucheksaraee and Chu, 2024). Zhou et al. (2025) developed a machine learning method combining ICESat-2 and Sentinel-2 to estimate SGLs depth and volume with improved accuracy over traditional methods. While SGL volume can be derived by remote sensing, these methods cannot distinguish between contributions from surrounding meltwater and bottom ablation. Additionally, the long revisit cycle of satellites limits detailed exploration of the dynamic evolution and life cycle of SGLs.

Model simulations provide a physical perspective on the formation and development of SGLs. However, there are relatively few studies on the SGL model, and current regional climate models (RCMs) do not account for SGLs. Nevertheless, initial efforts are underway to integrate SGLs into RCMs to assess their impact on surface mass balance (Timmermans and Fettweis, 2024). Some meltwater routing models focus on simulations of meltwater flow paths and filling destinations based on DEM and flow laws (Banwell et al., 2012; Leeson et al., 2012; Yang et al., 2018), yet they do not consider the energy transport within the SGLs and the resulting bottom ablation. Other models pay more attention to the vertical evolution process of SGLs based on surface energy balance. Lüthje et al. (2006) first developed a one-dimensional SGLs model with the enthalpy method solving phase changes, and a drainage model was incorporated to simulate horizontal expansion of SGL. Buzzard et al. (2018) incorporated ice lens formation and meltwater percolation in the firn to develop an SGL evolution model for Antarctic ice shelves. Law et al. (2020) proposed a novel one-dimensional energy-balance and phase transition SGLs model, named GlacierLake, which can simulate the multi-year evolution of SGLs in the GrIS ablation area. Nonetheless, some limitations remain in current models, notably concerning the parameterization of SGL albedo and the reliance on observed runoff input.

The albedo of SGLs is a pivotal parameter in the simulation of SGL evolution and determines the shortwave radiation budget. In all the models based on surface energy balance mentioned above, the albedo-depth parameterization stems from Lüthje et al. (2006) (hereafter L06), which was developed for sea ice melt ponds. Therefore, this parameterization may lead to an underestimation of SGL albedo (Lüthje et al., 2006) and an overestimation of bottom ablation. In-situ observations over several days showed the lake bottom ablation was 110–135 % of that in adjacent bare ice areas in southwest GrIS (Tedesco et al., 2012). Lüthje et al. (2006) conducted 30-day simulations in 1999 and 2001 that demonstrated a 110–170 % increase in the bottom ablation compared to the surrounding bare ice. Existing evidence of SGL-albedo feedback has been derived from short-term simulations and limited-duration observations. Furthermore, the input of surrounding meltwater in GlacierLake relies on in-situ observations and restricts the application of the model in areas without measurements.

To accurately estimate SGL bottom ablation and comprehensively understand the SGL-albedo feedback, in this study, we develop a new albedo-depth parameterization for SGLs using Sentinel-2 and ICESat-2 observations. A runoff module driven by in-situ atmospheric and snow measurements is then integrated into the updated SGLs model (GlacierLake_v2), which allows for a detailed examination of the bottom ablation process. Finally, we quantify the overall SGL-albedo feedback over the lifetime of SGL and explore the relationship between this feedback and lake depth.

2. Study area and data

2.1. Study area

The surface hydrologic system is particularly well-developed in central-west (CW) and southwestern (SW) GrIS (Fig. 1a), where SGLs cover approximately 50 % of the total SGLs area across the entire GrIS (Hu et al., 2022). Over the past four decades, the SGLs area in CW and SW basins has experienced significantly faster expansion rates (6.3 km^2 y^{-1} and 15.8 km^2 y^{-1}, respectively) compared to other basins (Fan et al., 2025). With detailed atmospheric and satellite observations, we chose 15 SGLs with Sentinel-2 and ICESat-2 observations on the same day in CW and SW basins (Fig. 1b), from which the albedo and depths are extracted to determine SGL albedo-depth parameterization. Except for southeastern and northeastern basins, we selected automatic weather stations (AWSs) with high-quality data and an appropriate temporal coverage to match satellite observations and the output of RCMs for assessing albedo and runoff (Fig. 1a). Lake BlueSnow (69.569 N, 49.342 W) is located close to Swiss Camp and reappears in approximately the same location almost every year (Fig. 1c). Detailed bottom ablation measurements of this lake were reported by Tedesco et al. (2012) and provide a valuable dataset for validating simulation results.

2.2. Sentinel-2 and Landsat 7 ETM+

Sentinel-2 is an Earth observation mission from the European Space Agency with two constellations (Sentinel-2A and Sentinel-2B) orbiting in tandem every 180°. It carries the MultiSpectral Instrument (MSI) that can capture 13 spectral bands at resolutions of 10 m, 20 m, and 60 m, respectively (ESA, 2024). Due to its high spatial resolution (10 m) in visible bands, Sentinel-2 has been extensively employed to extract hydrological elements on the GrIS surface (Williamson et al., 2018; Zhang et al., 2023). We searched SGLs on the GrIS using Level-2A surface reflectance products. The reflectance of the selected bands (B2, B3, B4, B8 at 10 m and B11, B12 at 20 m) is applied to calculate albedo, and the cloud mask in Sentinel-2 images uses the QA60 band. Landsat 7 was launched by NASA and the USGS on April 15, 1999. Equipped with the Enhanced Thematic Mapper Plus (ETM +) sensor, it provides multispectral and thermal infrared data for global land monitoring (Goward et al., 2001). In 2003, Landsat 7 experienced a failure of its Scan Line Corrector, which introduced scan-line artifacts into its imagery (El Fellah et al., 2017). With a spatial resolution of 30 m, Landsat 7 ETM + images were used to validate the date of SGL formation.

2.3. ICESat-2

ICESat-2 is a laser altimeter satellite launched by NASA in 2018. Its primary mission is to measure changes in the height of Earth's

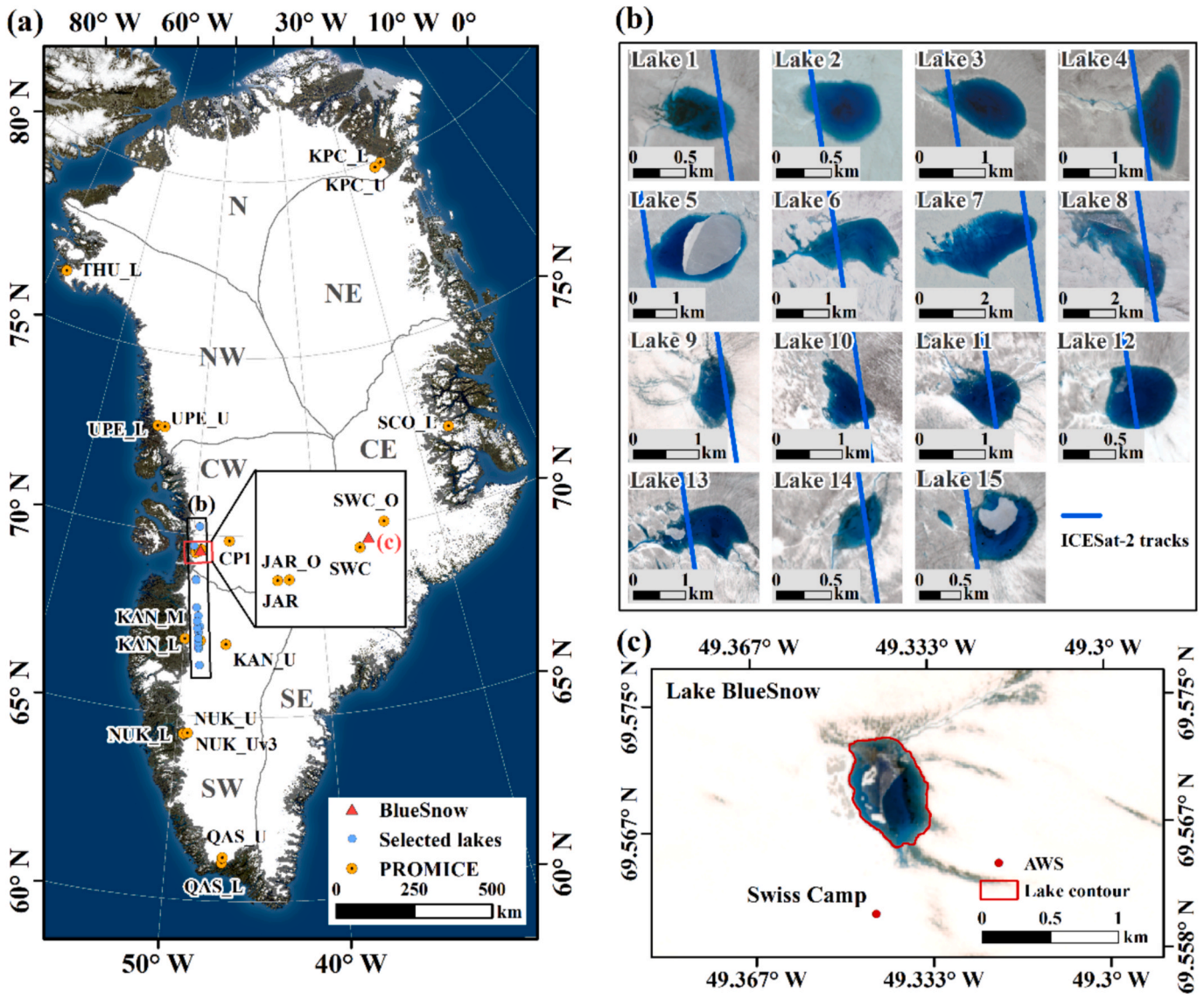

Fig. 1. (a) Map of Greenland showing the locations of automatic weather stations (AWSs) from PROMICE (yellow dots), selected supraglacial lakes (SGLs) crossed by ICESat-2 and Lake BlueSnow (highlighted with boxes and labeled "(b)" and "(c)", respectively). Base map is from Chen et al. (2020). (b) Details of ICESat-2 tracks (blue lines) crossing selected SGLs in central-west and southwest Greenland ice sheet. (c) Lake BlueSnow from Sentinel-2 on July 20, 2022, with the location of Swiss Camp indicated.

cryosphere, including ice sheets, glaciers, sea ice, and snow cover (Markus et al., 2017). It underpins many studies on surface mass balance (Smith et al., 2023), SGLs (Fricker et al., 2021), and even aerodynamic parameters (van Tiggelen et al., 2021). With a 91-day revisit cycle, ICESat-2 carries the Advanced Topographic Laser Altimeter System (ATLAS), which emits low-energy green photons (532 nm) at a frequency of 10 kHz (Neumann et al., 2019). ATLAS can divide a single laser pulse into six beams arranged in three pairs, each containing one strong beam and one weak beam. In the across-track direction, the distance between adjacent pairs is roughly 3.3 km, whereas the distance between the beams within each pair is approximately 90 m (Markus et al., 2017). ATL03 data record geolocated photon information, which includes precise longitude, latitude, elevation, photon signal confidence, and other related attributes (Neumann et al., 2022). It was validated by airborne LiDAR data in nearshore bathymetry, and within a depth range of 0 to −8.8 m, the RMSE ranges from 0.20-0.34 m (Albright and Glennie, 2021). Here, we use ATL03 data (strong beam) to get the lake depth. The true color images from Sentinel-2 of the selected SGLs and the ICESat-2 tracks are presented in Fig. 1b. Sentinel-2 and ICESat-2 data were collected on the same day, with details provided in Table S1.

2.4. *In-situ AWS and supraglacial lake observations*

The forcing and validation of the model heavily rely on the in-situ observations with high temporal resolution. The Greenland Climate Network (GC-Net) and the Programme for Monitoring of the Greenland Ice Sheet (PROMICE) have been continuously monitoring climate and ice sheet changes, with support from the Geological Survey of Denmark and Greenland (Fausto et al., 2021; Vandecrux et al., 2023). The AWSs measure basic meteorological variables including pressure, air temperature, wind speed and direction, relative humidity, downward and upward shortwave radiation fluxes, subsurface temperatures, and others. We used hourly data at Swiss Camp from GC-Net (Steffen et al., 2022) in 2010 to drive the SGL model. Additionally, hourly data from PROMICE (How et al., 2022) are employed to validate the albedo and drive model.

Currently, bottom ablation cannot be available via satellite observations and can only be obtained through in-situ measurements. In 2010, Tedesco et al. (2012) installed a device (two sensors fixed to a

stake) in Lake BlueSnow and measured bottom ablation, which is one of the few observations of SGLs on the GrIS. The bottom ablation data have been used in the validation of the improved SGL model in Law et al. (2020) and are also employed to evaluate the model performance in this study.

2.5. Outputs from regional climate models

While AWS can provide most of the driving data, it lacks measurements of precipitation and snowfall. The Regional Atmospheric Climate Model (RACMO2.3p2) and Modèle Atmosphérique Régional (MARv3.11.5) are developed to simulate the climate change and surface mass balance of polar ice sheets (Fettweis et al., 2017; van Meijgaard et al., 2008) and have been widely evaluated and proven to be well-suited for the GrIS (Huai et al., 2021; Leeson et al., 2018; Noël et al., 2016). Precipitation and snowfall data at a 1 km spatial resolution from RACMO2.3p2 are used to drive the GlacierLake_v2, and runoff outputs from RACMO2.3p2 and MARv3.11.5 are employed to validate the runoff simulated by GlacierLake_v2.

3. Methods

3.1. GlacierLake

The GlacierLake is a one-dimensional SGL model that can simulate the multi-year evolution of SGL. It divides the SGL evolution into five stages (1–5): bare ice, snow-covered ice, SGL, buried lake with/without snow, and surface melting of the buried lake. The model includes a snow module that applies the scheme from Essery (2015) to update snow parameters. The main model domain is divided into grids of constant size (0.1 m for the upper 15 m and 1 m below). Both the model stage and the state (ice, water, and slush) of each grid are determined by the enthalpy. Temporary lake grids with constant size are inserted into the main grid column to address height changes of the model domain with meltwater input. Backward-time and central-space method is used to estimate heat diffusion. The lake albedo is calculated using L06, as detailed in Section 3.2.3. Four-thirds rule is applied in the calculation of turbulent exchange at the upper and lower lake interfaces (Linden, 2000). For more information about the model, we refer readers to Law et al. (2020).

3.2. Supraglacial lake albedo-depth parameterization

3.2.1. Satellite-derived albedo with narrow-to-broadband conversion

Given the absence of direct albedo measurements on the SGL surface, albedo derived from satellite observations is employed instead. Narrow-to-broadband conversion is one of the prevalent methods for converting polar-orbiting satellite observations into broadband albedo (Qu et al., 2015). Liang (2000) summarized the conversion coefficients of various satellite sensors, including ASTER, AVHRR, ETM+/TM, and MODIS, among others. Li et al. (2018) derived conversion coefficients for Sentinel-2 over snow and snow-free surfaces based on a radiative transfer model. Subsequently, Bonafoni and Sekertekin (2020) determined the coefficients for Sentinel-2 MSI using a weighted method, which treats broadband albedo as an integral of narrowband reflectance. This method has been proven to be superior to that proposed by Li et al. (2018), and is therefore adopted to calculate albedo, as follows,

$$\alpha = \sum r_B{}^{*}\omega_B \tag{1}$$

where α is the surface broadband albedo, r_B represents the reflectance and ω_B is the weighting coefficient (Table S2) from Bonafoni and Sekertekin (2020).

To test the applicability of the conversion coefficients on GrIS, the derived albedo from Sentinel-2 is compared with in-situ measured albedo from PROMICE. First, we chose 10 AWSs (Table S3) around the selected SGLs, and filtered Sentinel-2 images with less than 50 % cloud coverage for each AWS. The matching of satellite images with AWS data in time and space is processed with reference to Feng et al. (2023). The time difference between the PROMICE records and satellite acquisitions was constrained to within 1 h. Within a 100 m spatial window (10 × 10 Sentinel-2 pixels), the averaged reflectance of each band was extracted using the annual mean coordinates of each AWS. Subsequently, the derived albedo from Sentinel-2 was calculated using Equation (1) and compared with the albedo measurements provided by PROMICE.

3.2.2. Lake depth extraction from ICESat-2

Although numerous automatic and semi-automatic algorithms exist for extracting lake depths, visual interpretation is still regarded as the most reliable method and is frequently employed to validate the accuracy of automatic extraction in existing studies (Fricker et al., 2021; Xiao et al., 2023). Delineating the lake surface and bottom is not time-consuming considering the limited number of selected SGLs. Therefore, the lake depths were obtained by visual interpretation. The ICESat-2 ATL03 file was loaded in PhotonLabeler, a graphical user interface that facilitates the labeling and visualization of ICESat-2 geolocated photons (Malambo and Popescu, 2020). Signal photons from the lake surface and the upper half of the lakebed in areas with high photon concentration were manually labeled and exported. Lake contours at the surface and bottom were determined by averaging photon elevations and calculating the lower envelope of photons, respectively, and the elevation difference between them defines the lake depth. We set the refraction coefficient of 1.33 to correct the overestimated depth due to the water refraction according to (Parrish et al., 2019),

$$ld_{cor} = \frac{ld}{1.33} \tag{2}$$

where ld and ld_{cor} are lake depths before and after correction, respectively.

3.2.3. Supraglacial lake albedo-depth parameterization

L06 is a widely used albedo-depth parameterization in SGLs modeling, developed based on observations from sea ice melt ponds, and shows a decaying exponential form,

$$\alpha = \frac{9702 + 1000e^{3.6h}}{-539 + 20000e^{3.6h}} \tag{3}$$

where α is the lake albedo and h is the lake depth. Early studies have shown that the albedo of melt ponds decays exponentially with depth (Ebert and Curry, 1993; Morassutti and LeDrew, 1996). The same variation was also reflected in spectral reflectance of SGLs from in-situ measurements, MODIS, and Sentinel-2 (Box and Ski, 2007; Lutz et al., 2024; Tedesco and Steiner, 2011; Williamson et al., 2018). The specific band values (B2, B3, B4, B8, B11, and B12) from Sentinel-2 were extracted along the ICESat-2 track of each SGL and were used to derive broadband albedo by Equation (1). We took exponential form to fit the albedo-depth curve based on the albedo and depth along the ICESat-2 tracks of the selected SGLs. The new albedo-depth parameterization is then integrated into the model and compared with the output results using L06 to assess its impact on simulation accuracy.

3.3. Runoff module incorporation

To provide the meltwater input for SGL, we added a meteorologically driven runoff module. Runoff is produced only when the first grid reaches the melting point. The maximum heat (Q_{max}, J) that can be released by refreezing all the liquid water (rainfall and meltwater) is given by,

$$Q_{max} = V\rho_{water}L_f \tag{4}$$

where V is the volume of liquid water (m^3), ρ_{water} is the density of water (1000 kg/m^3), and L_f is the latent heat of ice fusion (3.34 × 10^5 J kg^{-1}).

The energy required for the first grid to reach the melting point (Q_{change}, J) is calculated as follows,

$$Q_{change} = V_{ice}\rho_{ice}C(273.15 - T) \quad (5)$$

where V_{ice} is the volume of ice (m^3), ρ_{ice} is the density of ice (900 kg/m^3), and C is the specific heat capacity (J kg^{-1} K^{-1}). If $Q_{max} > Q_{change}$, the heat released by refreezing is sufficient to raise the first grid to the melting point, with any excess energy contributing to runoff generation. Conversely, the liquid water will completely refreeze (Buzzard, 2017).

The liquid water retention in the snowpack follows the scheme proposed by Coléou and Lesaffre (1998). The maximum water retention (W, %) in the snow layer (the percent of the snow layer mass) due to capillary is

$$W = 1.7 + 5.7^{*}\frac{P}{1-P} \quad (6)$$

$$P = 1 - \left(\frac{\rho_{snow}}{\rho_{ice}}\right) \quad (7)$$

where P is the snow porosity, ρ_{snow} is the density of snow (kg/m^3).

3.4. GlacierLake_v2

The improved version of GlacierLake (GlacierLake_v2) is implemented by a newly developed albedo-depth parameterization, additional runoff and spin-up modules (Fig. S1). The spin-up module is incorporated into the model, outputting surface temperature and snow properties as initial conditions, and the output of the runoff module will serve as the meltwater input to the main module. Additionally, we have made minor adjustments to the original code to resolve runtime errors that occurred under specific conditions.

GlacierLake_v2 employs the same approach as GlacierLake for computing energy exchange within the model domain. The model was forced with downward shortwave radiation, downward longwave radiation, albedo, air temperature, pressure, wind speed, relative humidity, precipitation, and snowfall. All variables were obtained from the AWS at Swiss Camp, except for precipitation and snowfall, which were provided by the RACMO2.3p2. To evaluate the performance of GlacierLake_v2, two sets of comparative experiments were conducted. First, the model was run using the original hydrological inputs, coupled separately with the original and new albedo-depth parameterizations. Due to the limited observation period of the original hydrological data, the simulation was restricted to 6 days. Subsequently, the runoff module was used to provide the meltwater input, again coupled with both albedo parameterizations. In this case, the simulation started on January 1, 2010, and covered one year.

3.5. Quantification of supraglacial lake-albedo feedback

The SGLs exhibit a lower albedo than the surrounding bare ice, leading to enhanced absorption of downward shortwave radiation and a corresponding increase in melt. The relative difference in melt rate between lake and bare ice is used to quantify the SGL-albedo feedback (%),

$$feedback = \frac{M_{lake} - M_{ice}}{M_{ice}} \times 100\% \quad (8)$$

where M_{lake} and M_{ice} represent the melt rate from SGLs and the surrounding bare ice, respectively.

The framework of this study is shown in Fig. 2. We developed a new albedo-depth parameterization using lake depth extracted from ICESat-2 and lake albedo derived from Sentinel-2 through narrow-to-broadband conversion. The conversion coefficient was validated against measured albedo from AWSs. A runoff module was developed to provide the meltwater input for SGLs. We used observed meteorological data from PROMICE to drive the runoff module and compared the simulated results to the RCMs. The new albedo-depth parameterization and runoff module were incorporated into GlacierLake_v2, which we used to simulate the evolution of Lake BlueSnow. The measured bottom ablation of Lake BlueSnow was employed to evaluate the simulation performance, and the SGL-albedo feedback was quantified.

4. Result

4.1. Improved supraglacial lake albedo-depth parameterization

We used measured albedo from PROMICE to verify the applicability of the narrow-to-broadband conversion approach in GrIS. Overall, the satellite-derived albedo agrees well with the measurement from AWSs (Fig. S2), as indicated by an R^2 of 0.645 and an *RMSE* of 0.116. The

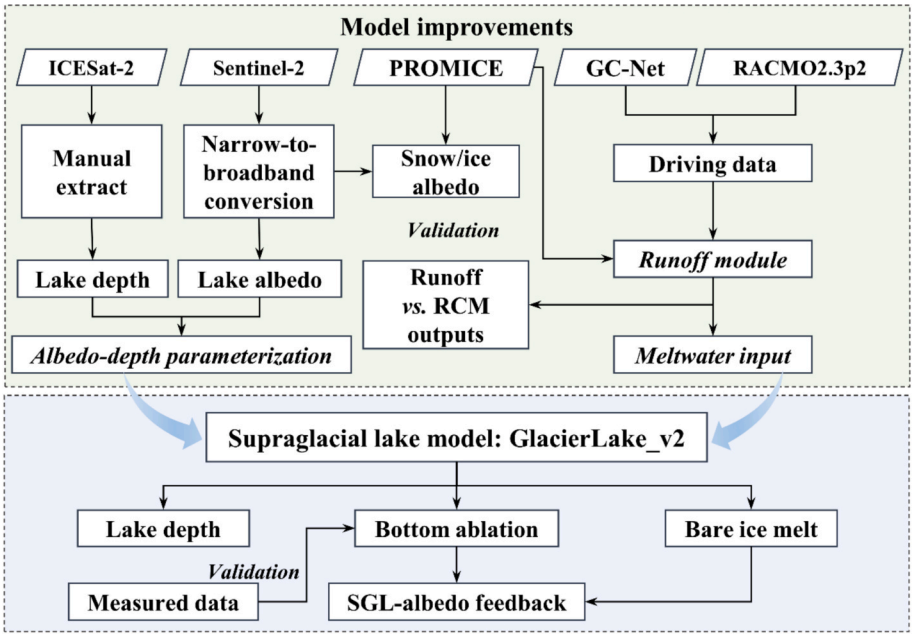

Fig. 2. The framework of this study.

predicted albedo shows a slight overestimation compared to observed values, with a bias of 0.035. However, albedo is underestimated in the high albedo range (0.8–1). Given the characteristically low albedo of SGLs, the narrow-to-broadband conversion method is appropriate for deriving their albedo.

The surface and bottom contours of the selected SGLs were manually extracted through visual interpretation (Fig. 3) to avoid errors introduced by automatic processing. Lake depths were determined by the elevation difference between the surface and bottom. After the correction of water refraction, mean depths ranged from 1.15 m to 3.8 m. Lake 8 was the deepest, with a mean depth of 3.8 m and a maximum depth of 9.11 m, while Lake 14 had the shallowest mean depth of 1.15 m.

Albedo-depth curve was finally determined to a three-parameter form, which demonstrated the best statistical indexes (R^2, *RMSE*, *BIAS*) and is consistent with the form derived by Ebert and Curry (1993),

$$\alpha = b + exp(ch + d) \quad (9)$$

where α is the albedo of SGLs, h is the lake depth, b=0.1911, c=-1.0445, d=-0.9183. The variation of albedo with depth can be well reproduced by the newly developed parameterization (Fig. 4), with an R^2 of 0.81 and an *RMSE* of 0.04, while L06 significantly underestimates the overall albedo. The albedo from L06 decreases rapidly with depth from 0 to 1.5 m, after which it reaches a constant value of 0.05. However, the new parameterization indicates that the albedo decreases significantly within 0 to 2 m, approaching a constant value of 0.19 at depths beyond 4 m.

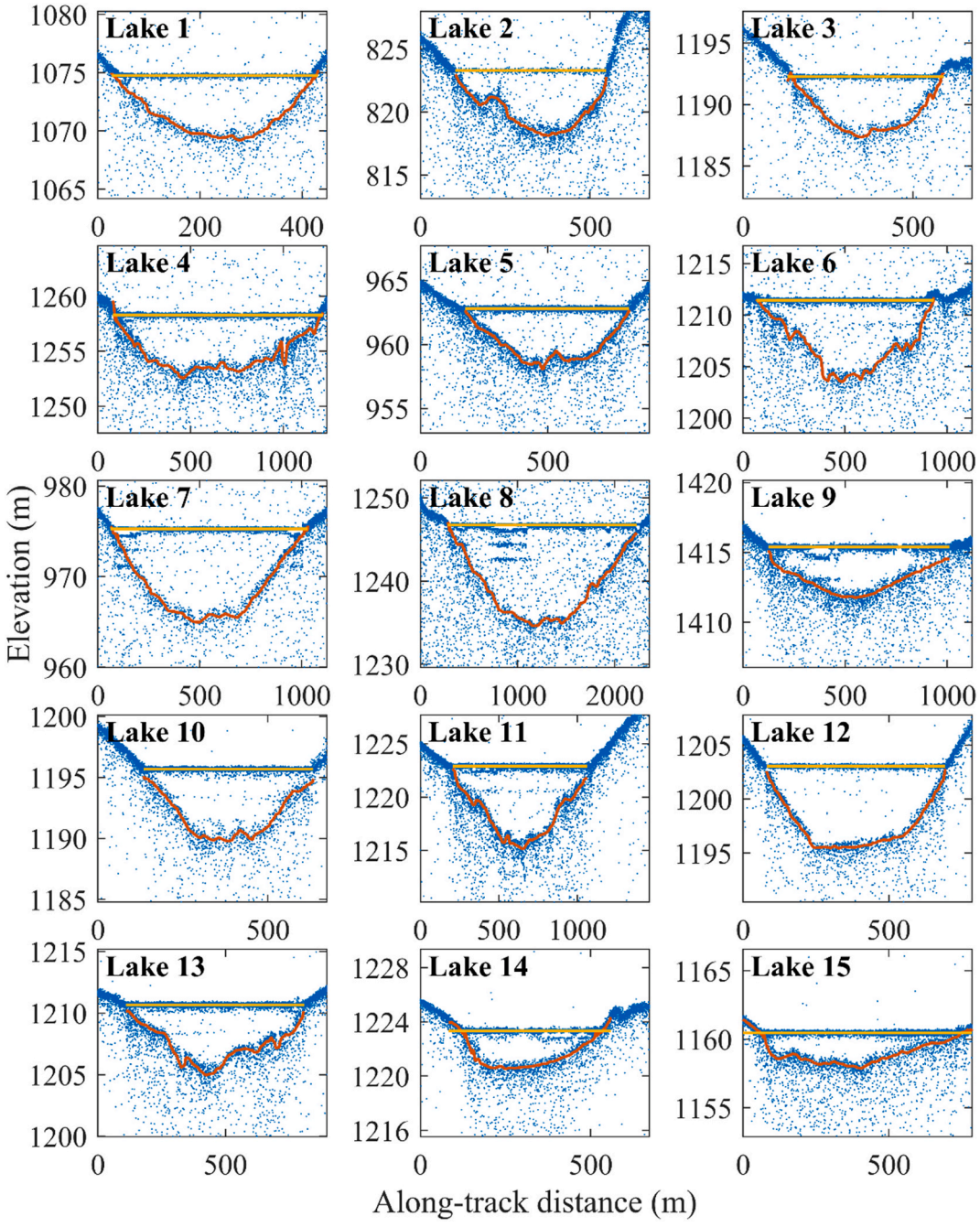

Fig. 3. Manual extraction of the outline of the selected SGLs. The blue dots are ICESat-2 photons, the yellow and red lines represent the lake surface and bed, respectively.

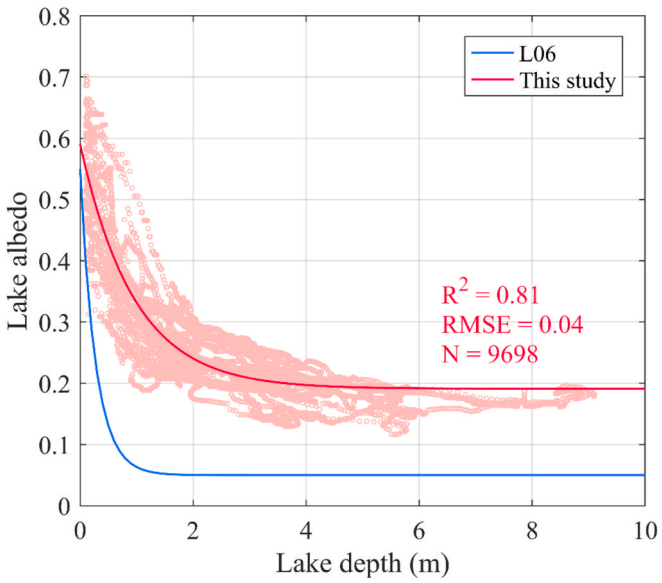

Fig. 4. Comparison between the proposed albedo-depth parameterization (red) and L06 (blue).

4.2. Comparison between AWS-derived and RCM-simulated runoff

We selected 12 PROMICE AWSs with long observation periods and high data continuity (Table S3). The measurement data from AWSs were used to drive runoff estimates, which were then compared with runoff outputs from RCMs. Overall, meltwater runoff is well reproduced by RCMs, with R^2 values of 0.65 and 0.63 for RACMO2.3p2 and MARv3.11.5, respectively (Fig. 5). RACMO2.3p2 is slightly outperforming MARv3.11.5, with a lower *RMSE* of 0.92 m w.e. yr^{-1} and a bias of 0.25 m w.e. yr^{-1}, while MARv3.11.5 exhibits a negative bias of 0.32 m w.e. yr^{-1}. Regionally, except for SCO_L and KPC_U, the RCM-derived runoff is positively correlated with the AWS-derived runoff at other sites, and a significantly strong positive correlation exists in the SW basin (Fig. S3a). However, RACMO2.3p2 shows a significant overestimation at the southernmost QAS_U, while MARv3.11.5 exhibits the opposite. Specifically, RCMs demonstrate favorable performance at the KAN_L ($r = 0.91$ for MAR v3.11.5, $r = 0.95$ for RACMO2.3p2, $p < 0.05$, Fig. S3a), with smaller *RMSEs* of 0.28 and 0.27 m w.e. yr^{-1} (Fig. S3b), and biases of 0.15 and 0.18 m w.e. yr^{-1} (Fig. S3c). In contrast, runoff

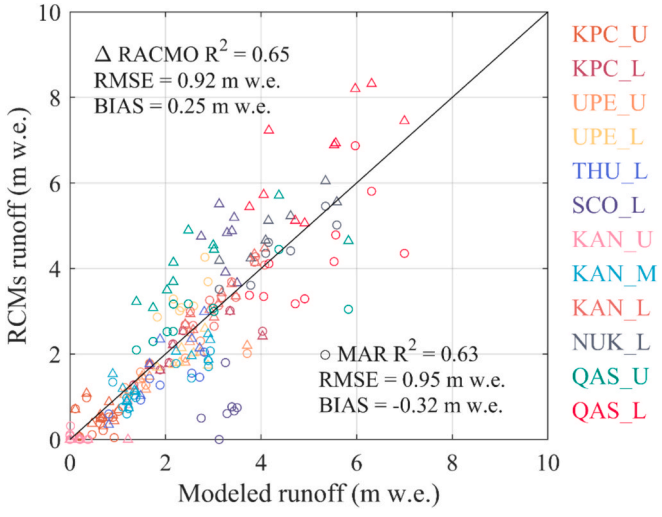

Fig. 5. Comparison between simulated runoff from the AWS observations and the RCMs outputs.

from RCMs show a negative correlation with AWS-derived runoff at SCO_L, and RACMO2.3p2 and MAR v3.11.5 greatly overestimated and underestimated runoff, respectively.

4.3. Model verification and evolution of supraglacial lake from GlacierLake_v2

Newly developed albedo-depth parameterization and the runoff module were validated by comparing bottom ablation between the model output and in-situ measurement in Lake BlueSnow. First, a 6-day (DOY 175 to 180) simulation was performed, with initial lake depth and water temperature from Tedesco et al. (2012), and the original hydrological input was used. Bottom ablations simulated by using L06 and the new parameterization were shown in Fig. 6a. Bottom ablation was overestimated by L06 (*BIAS* = 2.59 cm). The new parameterization mitigated this overestimation (*BIAS* = 0.49 cm) and demonstrated superior performance compared to L06, with a higher R^2 of 0.95 and a reduction in *RMSE* by 1.97 cm. Subsequently, the runoff module replaced the original hydrological input. The model was run for one year from January 1, 2010, with initial inputs provided by the spin-up module. Simulations were conducted using L06 and the new parameterization, respectively. As shown in Fig. 6b, the simulation result for L06 also exhibited an overestimation (*BIAS* = 2.66 cm), while the bottom ablation simulated with the new parameterization is in close agreement with in-situ measurements (R^2 = 0.98, *RMSE* = 1.19 cm, *BIAS* = -0.36 cm). Compared to the original hydrologic input and L06 (GlacierLake), the *RMSE* was reduced by 2.46 cm when using the runoff module and the new parameterization (GlacierLake_v2). These results demonstrate that GlacierLake_v2 is excellent at simulating bottom ablation.

In Fig. 6b, only the simulated bottom ablations during the period with in-situ measurements were presented, while the full one-year lake evolution simulations are displayed in Fig. 7. The simulations using L06 and the new parameterization are referred to as G2P1 and G2P2, respectively. The initial snow depth was 1.05 m after spin-up. Following snowfall accumulation from January to April, it reached a maximum of 1.71 m on May 1 (Fig. 7b and 7e). The absorbed energy was mainly used to melt the thicker snow cover in May, which delayed the formation of SGL until June 3 (Fig. 7c and 7f). During the SGL period (June 4 to September 9), the energy budget of G2P1 is 30 % higher than that of G2P2. The maximum lake depth simulated by G2P2 was 5.65 m, which was 1.08 m shallower than that simulated by G2P1. With the temperature decrease, the SGL surface began to freeze from September 10 (Fig. 7c and 7f), leading to the formation of a buried lake. Due to the reduced energy budget and lower ice temperatures below the lake, the lake bottom began to freeze after the formation of the buried lake. By December 31, the thickness of the ice lid and the bottom freeze from G2P2 were approximately 2 m and 0.19 m, respectively.

4.4. Quantification of supraglacial lake-albedo feedback

Based on the simulations from G2P2, the relationship between the SGL-albedo feedback and lake depth is displayed in Fig. 8a. SGL-albedo feedback decreased overall with increasing lake depth. High feedback values (gray shading) appeared intermittently, particularly extreme on June 16 and September 6 (red cycles), which coincided with snowfall events (Fig. 8c). Snowfall rapidly increased the bare ice albedo, leading to a significant reduction in the melt rate or a complete cessation of melting (Fig. 8b). In general, the bare ice melt rate was relatively low at the onset of melting season, corresponding to higher feedback, and then the feedback exponentially decreased with the lake depth. When the lake depth reached 2–4 m (in July), the feedback markedly decreased. During this period, changes in lake depth had an insignificant effect on lake albedo (from 0.25 to 0.20), while the reduction in downward shortwave radiation led to a lower lake melt rate. At the same time, the bare ice albedo rapidly decreased from 0.74 to 0.31, causing a

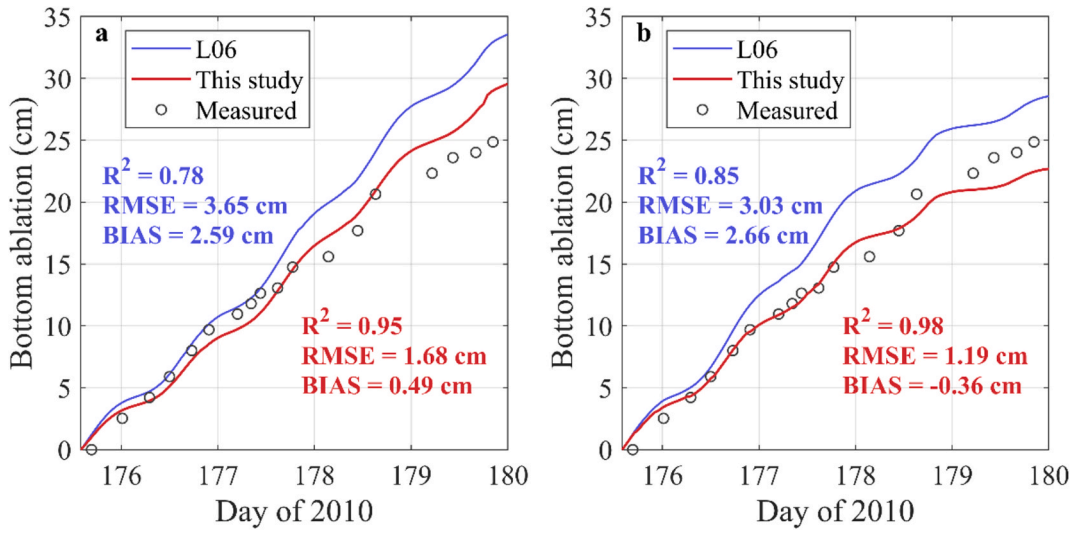

Fig. 6. With original hydrological input (a) and runoff module (b), comparison of measured and simulated bottom ablation using original and new albedo-depth parameterization, respectively.

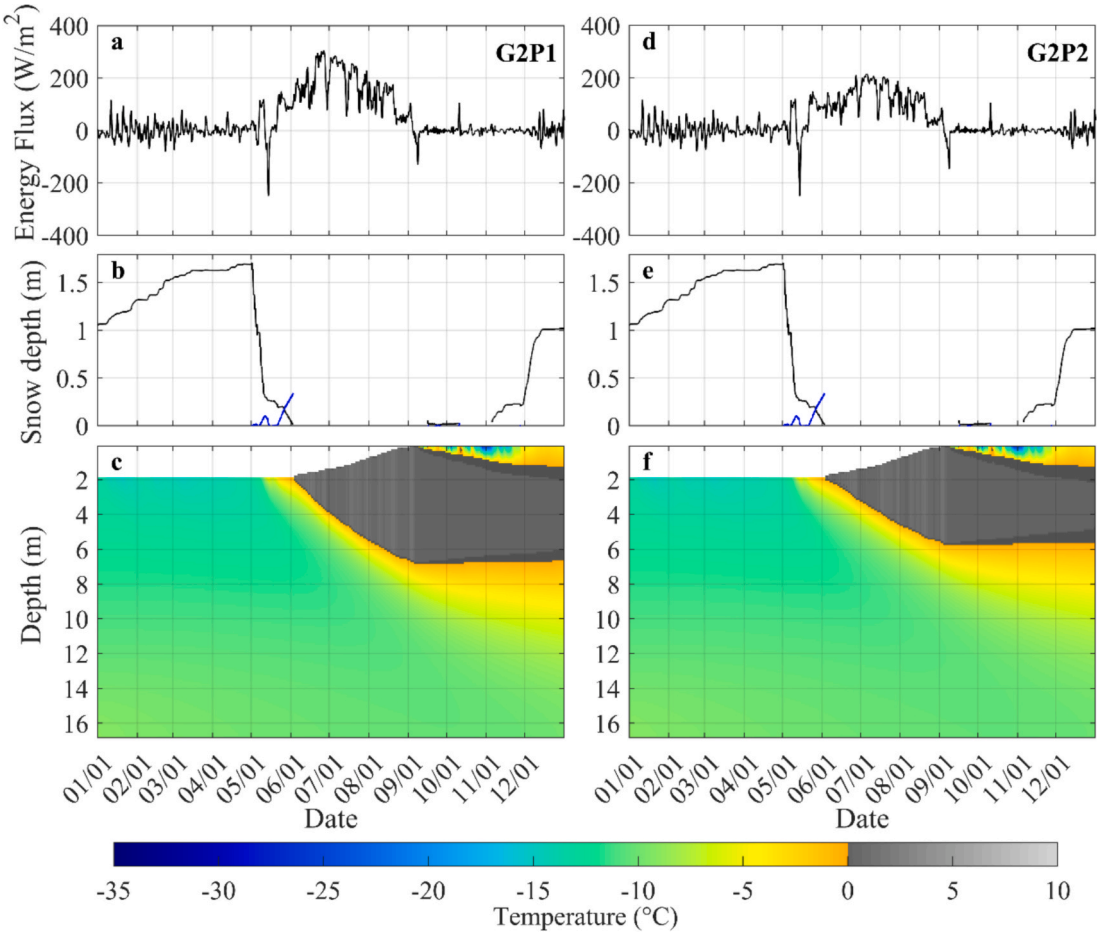

Fig. 7. Comparison of the evolution process of Lake BlueSnow for G2P1 and G2P2. (a, d) 24-hour moving average of the hourly surface energy budget, (b, e) snow depth (black line) and water depth in the snow layer (blue line), and (c, f) temperature of the model domain, the darker gray areas represent slush, its enthalpy lies between that of water and ice.

significant increase in the bare ice melting rate, which led to a subsequent decrease in feedback. The mean melt rate of the lake is 4 cm d^{-1}, which is 2.2 times stronger than that of bare ice with the lake-albedo feedback.

5. Discussion

In this study, we developed a new albedo-depth parameterization based on satellite observations, which significantly outperforms the

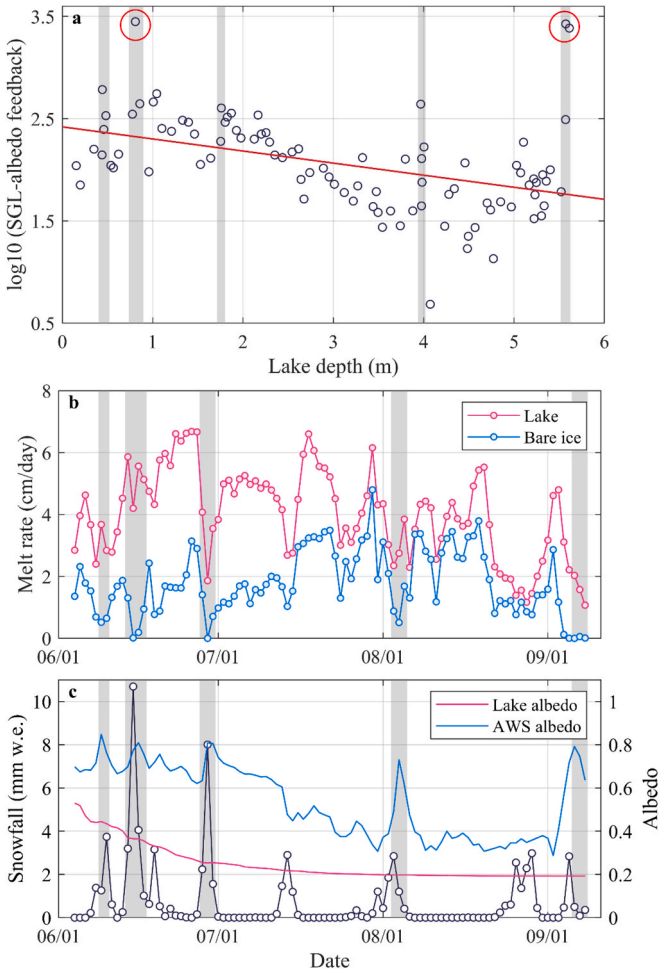

Fig. 8. (a) Relationship between SGL-albedo feedback and lake depth. Extremely high feedback is highlighted with red circles, and the regression is shown as a red line. (b) The daily melt rates of Lake BlueSnow (pink) and bare ice (blue). (c) The snowfall at Swiss Camp from RACMO2.3p2, and lake albedo (pink) and AWS albedo (blue) from PROMICE. Gray shadings are used to highlight the snowfall events and the resulting increase in albedo, decrease in bare ice melt rate, and higher feedback around June 9, June 16, June 29, August 4, and September 6.

widely used L06. L06 was developed based on measured optical data and depth of sea ice melt ponds. The melt ponds are shallower than SGLs, and the difference in water quality (i.e., salinity) results in greater absorption at specific wavelengths (Pegau et al., 1997) and increased scattering (Smith and Baker, 1981). Therefore, L06 generally underestimates albedo when applied to SGLs modeling. The lake albedo used for developing the new parameterization was obtained through narrow-to-broadband conversion. Although this method has gained widespread recognition (Bonafoni and Sekertekin, 2020; Du et al., 2023; Feng et al., 2023), the absence of in-situ observations over SGLs poses challenges in validating the applicability of narrow-to-broadband conversion coefficients for SGLs. When applying the narrow-to-broadband conversion method, it is typically necessary to assume a Lambertian surface (Bonafoni and Sekertekin, 2020; Du et al., 2023). However, SGLs are non-ideal Lambertian reflectors, exhibiting both specular reflection and light transmission. Consequently, the lake surface was treated as a Lambertian reflector for simplification, which may lead to an overestimation of albedo. Currently, measurements of SGLs reflectance are limited to visible and near-infrared bands (Box and Ski, 2007; Tedesco and Steiner, 2011), with a maximum wavelength of 1025 nm. However, the lake albedo derived from the narrow-to-broadband conversion involves Sentinel-2 shortwave infrared bands, which extend up to 2280 nm. Therefore, the current in-situ measurements are insufficient to support the validation of our parameterization, and more comprehensive field measurements of SGLs reflectance across a broader spectral range are required to enable robust validation. In Fig. S2, we assessed the applicability of the conversion coefficients for GrIS, showing that the albedo is underestimated in the high-albedo range (0.8–1). Feng et al. (2023) found a similar underestimation in GrIS, attributing it to the larger footprint of the satellite, which captures more snow-free areas than AWS measurements.

The fact that deeper water absorbs more solar radiation and thus exhibits lower reflectance forms the theoretical basis for remote sensing-based lake depth retrieval (Pope et al., 2016). Most existing studies in western GrIS have derived empirical relationships between lake depth and reflectance based on samples from only one or two lakes (Box and Ski, 2007; Fitzpatrick et al., 2014; Tedesco and Steiner, 2011), leading to strong regional dependence. Lutz et al. (2024) derived reflectance-depth equations by combining ICESat-2-derived lake depths and Sentinel-2 reflectance data from southwestern and northeastern GrIS. Their results show that, at the same depth and within the same spectral band, lakes in northeastern GrIS exhibit higher reflectance than those in the southwest, likely due to the widespread presence of dark bottom sediments in the latter. This also presents a challenge for the application of newly developed albedo-depth parameterizations to SGLs in northeastern GrIS.

Measured meltwater inputs are required in the GlacierLake model. A drainage model based on the DEM and the tuning topographic parameter was employed to simulate the meltwater lateral transport (Lüthje et al., 2006). Buzzard et al. (2018) developed the one-dimensional SGL model for the Larsen C ice shelf in Antarctica, with a separate firn column model to output meltwater. Law et al. (2020) used a measured hydrograph by Tedesco et al. (2012) in Lake BlueSnow, with the record covering only a few days. To apply the GlacierLake model to lakes without observation, we incorporated a meteorologically driven runoff module, with its runoff output serving as the meltwater input to the SGL. In Fig. 5, we used observed data from PROMICE to drive the module and compared the simulated results to the output of RCMs. Notably, at the KAN_U (1823 m) in the Southwest Basin, RACMO2.3p2 simulated no runoff (Fig. 5). This means that the RCMs may underestimate the runoff limit in certain areas, which is also evidenced in recent comparisons between optical images and RACMO2.3p2 output (Zhang et al., 2023).

We used optical imagery to assist in the validation of the model. Based on Landsat 7 images from 2010 (Table S4), no lake formation was observed by May 29 (Fig. S4a). However, limited by the revisit cycle, Lake BlueSnow had already formed by the next available image on June 7 (Fig. S4b). The simulated lake formation date of June 3 falls within this interval, demonstrating consistency with the satellite observation. Currently, the estimation of bottom ablation relies heavily on models, and research on bottom ablation remains far less developed compared to studies on lake extraction and the retrieval of lake depth and volume. Tedesco et al. (2012) simulated the bottom ablation of Lake BlueSnow, reporting an *RMSE* of 4.7 cm. In contrast, the improved GlacierLake_v2, incorporating the new albedo-depth parameterization and runoff module, achieved a significantly lower *RMSE* of only 1.2 cm, representing a reduction of 3.5 cm. However, the evaluation is limited by the short duration of available in-situ observations and the fact that the comparison was conducted at Lake BlueSnow. This temporal and spatial constraint may influence the representativeness of the performance indexes. Additionally, as a one-dimensional column model, GlacierLake_v2 simulates the vertical energy balance, while the observed bottom ablation used for validation reflects real-world three-dimensional lake conditions, including lateral energy inputs and convective mixing. Therefore, the current assumption of no lateral energy exchange may introduce some uncertainty. The next step is to extend the model to two dimensions, enabling representation of lateral flow and spatial heterogeneity in SGL development.

Summer snowfall-induced albedo surges can temporarily slow the

melt rate of bare ice through the snow albedo-melt feedback mechanism (Noël et al., 2015). However, the presence of SGLs may negate this feedback. In Fig. 8c, high feedback coincided with significant snowfall. AWS albedo sharply increases with fresh snow, resulting in a reduction in bare ice melt rates. However, snowfall did not alter lake albedo, leading to an increase in SGL-albedo feedback. Under global warming, artificial snow enhancement has been proposed to mitigate future ice sheet mass loss (Feldmann et al., 2019; Fettweis et al., 2021); nevertheless, the presence of SGLs may undermine the effectiveness of such interventions.

With continued climate warming, SGLs are likely to grow larger and deeper. Leeson et al. (2015) simulated the growth of SGLs on the SW GrIS under both present (1971–2010) and future scenarios (2011–2060, RCP4.5 and RCP8.5), showing that mean lake size increased 13 %-20 %. The current albedo-depth parameterization may not be fully applicable under future scenarios. However, the lake albedo becomes insensitive to further increases in lake depth once a certain threshold is reached, suggesting that the impact may be limited. Additionally, the dust and black carbon deposited on the GrIS surface have been proven to decrease ice albedo (Goelles and Bøggild, 2017). Snow and ice algae blooms have attracted widespread attention due to their ability to reduce surface albedo, which in turn intensifies surface melting (Cook et al., 2020; Onuma et al., 2018; Williamson et al., 2020), and their effect on bare ice darkening is more pronounced compared to non-algal impurities (Stibal et al., 2017). These impurities may alter the physical properties of SGLs, in particular, as the presence of liquid water can promote algal growth (Tedstone et al., 2020), thereby introducing additional uncertainty into the current albedo-depth parameterization.

Our results provide new insights into the SGL-albedo feedback mechanisms, which are essential for refining projections of future SGL behavior under warming scenarios. GlacierLake_v2 establishes a foundation for future two- and three-dimensional modeling of SGL evolution and can also be integrated as a module into the model of ice flow, crevasses, and subglacial hydrology. We hope to extend the application of this model to mountain glacier regions, such as High Mountain Asia, to assess its capability in predicting glacial lake outburst events. A more comprehensive supraglacial hydrological model needs lateral and basal drainage processes, which are not yet incorporated into the current model and represent an important direction for future improvements.

6. Conclusion

This study presented an improved SGL model (GlacierLake_v2) that enhances the simulation of bottom ablation by integrating a novel albedo-depth parameterization and a meteorologically driven runoff module, and quantified the SGL-albedo feedback. The proposed albedo-depth parameterization based on ICESat-2 and Sentinel-2 accurately captures the relationship between lake albedo and depth ($R^2 = 0.81$), overcoming the albedo underestimation in L06. While RCM-derived runoff generally aligns with that from the AWS-driven runoff module, significant biases persist in the southern margins of GrIS, where the inability of coarse-resolution RCMs to capture complex local terrain may be a contributing factor. GlacierLake_v2 significantly improves bottom ablation simulation accuracy, reducing *RMSE* by 67 % compared to GlacierLake.

The SGL-albedo feedback is jointly controlled by the melt rates of the lake bottom and bare ice. Sudden snowfall events during the melt season can sharply reduce or even eliminate surface melt. In July, when snowfall is infrequent, the rapid increase in bare ice melt leads to declining feedback. In contrast, snowfall events in June and August result in abrupt increases in feedback, highlighting the strong regulatory role of SGL in the surface energy balance. The findings of this study contribute significantly to advancing the understanding of surface melt processes on the GrIS, the development of SGLs, and the associated albedo feedback mechanisms. Integrating GlacierLake_v2 into RCMs has the potential to reduce uncertainties in the estimates of surface mass loss, thereby improving projections of global sea-level rise.

CRediT authorship contribution statement

Jiake Wu: Writing – original draft, Visualization, Validation, Software, Methodology, Investigation, Formal analysis, Data curation. **Lei Zheng:** Writing – review & editing, Supervision, Methodology, Investigation, Funding acquisition, Formal analysis, Conceptualization. **Zhuoqi Chen:** Methodology, Investigation. **Quan Zhou:** Validation, Methodology, Data curation. **Chuyue Peng:** Software, Investigation. **Qi Liang:** Validation, Investigation. **Teng Li:** Investigation, Formal analysis. **Baojuan Huai:** Investigation, Data curation. **Weijun Sun:** Investigation, Data curation. **Xiao Cheng:** Supervision, Resources, Funding acquisition. **Robert Law:** Writing – review & editing, Software, Formal analysis. **Fengming Hui:** Writing – review & editing, Validation, Supervision, Methodology, Investigation, Conceptualization.

Declaration of competing interest

The authors declare that they have no known competing financial interests or personal relationships that could have appeared to influence the work reported in this paper.

Acknowledgments

This study was supported by the National Natural Science Foundation of China (Grant Nos. 42422606 and 42476256) and the Guangdong Basic and Applied Basic Research Foundation (2021B1515020032). We especially thank Dr. Raul-David Serban for the English editing.

Appendix A. Supplementary material

Supplementary data to this article can be found online at https://doi.org/10.1016/j.jhydrol.2025.134001.

Data availability

The GlacierLake_v2 code can be found at https://github.com/Jiake404/GlacierLake_v2/.

The Sentinel-2 datasets are sourced from ESA (https://dataspace.copernicus.eu/, accessed on October 19, 2023). The Landsat 7 ETM + datasets are obtained from USGS (https://earthexplorer.usgs.gov/, accessed on February 19, 2025). The ICESat-2 dataset is provided by NASA (https://nsidc.org/data/atl03/versions/6, accessed on October 19, 2023). The PROMICE and GC-NET datasets are available from GEUS at https://dataverse.geus.dk/dataset.xhtml?persistentId=doi:10.22008/FK2/IW73UU and https://dataverse.geus.dk/dataset.xhtml?persistentId=doi:10.22008/FK2/VVXGUT (accessed on November 11, 2023), respectively. The RACMO2.3p2 dataset is provided by Dr. Brice Noël (University of Liège), and the MAR dataset is provided by Dr. Xavier Fettweis (University of Liège) and accessed from http://phypc15.geo.ulg.ac.be/fettweis/MARv3.11/Greenland/ERA5_1950-2020-10km/daily_10km/ (accessed on July 1, 2024).

References

Ahmadianfar, I., Samadi-Koucheksaraee, A., Asadzadeh, M., 2022. Extract nonlinear operating rules of multi-reservoir systems using an efficient optimization method. Sci. Rep. 12, 18880. https://doi.org/10.1038/s41598-022-21635-0.

Albright, A., Glennie, C., 2021. Nearshore bathymetry from fusion of Sentinel-2 and ICESat-2 observations. IEEE Geosci. Remote Sens. Lett. 18, 900–904. https://doi.org/10.1109/LGRS.2020.2987778.

Arndt, P.S., Fricker, H.A., 2024. A framework for automated supraglacial lake detection and depth retrieval in ICESat-2 photon data across the Greenland and Antarctic ice sheets. Cryosphere 18, 5173–5206. https://doi.org/10.5194/tc-18-5173-2024.

Asadi, M., Sarabi, S., Kordani, M., Ilani, M.A., Banad, Y.M., 2025. Enhanced-HisSegNet: improved SAR image flood segmentation with learnable histogram layers and active

contour model. IEEE Geosci. Remote Sens. Lett. 22, 1–5. https://doi.org/10.1109/LGRS.2025.3532334.
Banwell, A.F., Arnold, N.S., Willis, I.C., Tedesco, M., Ahlstrøm, A.P., 2012. Modeling supraglacial water routing and lake filling on the Greenland Ice Sheet. J. Geophys. Res. Earth Surf. 117, F04012. https://doi.org/10.1029/2012JF002393.
Bonafoni, S., Sekertekin, A., 2020. Albedo retrieval from Sentinel-2 by new narrow-to-broadband conversion coefficients. IEEE Geosci. Remote Sens. Lett. 17, 1618–1622. https://doi.org/10.1109/LGRS.2020.2967085.
Box, J.E., Ski, K., 2007. Remote sounding of Greenland supraglacial melt lakes: implications for subglacial hydraulics. J. Glaciol. 53, 257–265. https://doi.org/10.3189/172756507782202883.
Buzzard, S.C., 2017. Modelling melt lake formation on an ice shelf. UNIVERSITY OF READING.
Buzzard, S.C., Feltham, D.L., Flocco, D., 2018. A mathematical model of melt lake development on an ice shelf. J. Adv. Model. Earth Syst. 10, 262–283. https://doi.org/10.1002/2017MS001155.
Chen, Z., Chi, Z., Zinglersen, K., Tian, Y., Wang, K., Hui, F., Cheng, X., 2020. A new image mosaic of Greenland using Landsat-8 OLI images. Sci. Bull. 65. https://doi.org/10.1016/j.scib.2020.01.014.
Chudley, T.R., Christoffersen, P., Doyle, S.H., Bougamont, M., Schoonman, C.M., Hubbard, B., James, M.R., 2019. Supraglacial lake drainage at a fast-flowing Greenlandic outlet glacier. PNAS 116, 25468–25477. https://doi.org/10.1073/pnas.1913685116.
Coléou, C., Lesaffre, B., 1998. Irreducible water saturation in snow: experimental results in a cold laboratory. Ann. Glaciol. 26, 64–68. https://doi.org/10.3189/1998AoG26-1-64-68.
Cook, J.M., Tedstone, A.J., Williamson, C., McCutcheon, J., Hodson, A.J., Dayal, A., Skiles, M., Hofer, S., Bryant, R., McAree, O., McGonigle, A., Ryan, J., Anesio, A.M., Irvine-Fynn, T.D.L., Hubbard, A., Hanna, E., Flanner, M., Mayanna, S., Benning, L.G., van As, D., Yallop, M., McQuaid, J.B., Gribbin, T., Tranter, M., 2020. Glacier algae accelerate melt rates on the south-western Greenland Ice Sheet. Cryosphere 14, 309–330. https://doi.org/10.5194/tc-14-309-2020.
Datta, R.T., Wouters, B., 2021. Supraglacial lake bathymetry automatically derived from ICESat-2 constraining lake depth estimates from multi-source satellite imagery. Cryosphere 15, 5115–5132. https://doi.org/10.5194/tc-15-5115-2021.
Du, J., Zhou, H., Jacinthe, P.-A., Song, K., 2023. Retrieval of lake water surface albedo from Sentinel-2 remote sensing imagery. J. Hydrol. 617, 128904. https://doi.org/10.1016/j.jhydrol.2022.128904.
Ebert, E.E., Curry, J.A., 1993. An intermediate one-dimensional thermodynamic sea ice model for investigating ice-atmosphere interactions. J. Geophys. Res. Oceans 98, 10085–10109. https://doi.org/10.1029/93JC00656.
El Fellah, S., Rziza, M., El Haziti, M., 2017. An efficient approach for filling gaps in Landsat 7 satellite images. IEEE Geosci. Remote Sens. Lett. 14, 62–66. https://doi.org/10.1109/LGRS.2016.2626138.
ESA, 2024. Sentinel-2 MSI User Guide [WWW Document]. URL https://sentinel.esa.int/web/sentinel/user-guides/sentinel-2-msi (accessed 5.14.24).
Essery, R., 2015. A factorial snowpack model (FSM 1.0). Geosci. Model Dev. 8, 3867–3876. https://doi.org/10.5194/gmd-8-3867-2015.
Fan, Y., Ke, C.-Q., Luo, L., Shen, X., Livingstone, S.J., Lea, J.M., 2025. Expansion of supraglacial lake area, volume and extent on the Greenland ice sheet from 1985 to 2023. J. Glaciol. 71, 1–13. https://doi.org/10.1017/jog.2024.87.
Fausto, R.S., van As, D., Mankoff, K.D., Vandecrux, B., Citterio, M., Ahlstrøm, A.P., Andersen, S.B., Colgan, W., Karlsson, N.B., Kjeldsen, K.K., Korsgaard, N.J., Larsen, S. H., Nielsen, S., Pedersen, A.Ø., Shields, C.L., Solgaard, A.M., Box, J.E., 2021. Programme for monitoring of the Greenland Ice Sheet (PROMICE) automatic weather station data. Earth Syst. Sci. Data. 13, 3819–3845. https://doi.org/10.5194/essd-13-3819-2021.
Feldmann, J., Levermann, A., Mengel, M., 2019. Stabilizing the West Antarctic Ice Sheet by surface mass deposition. Sci. Adv. 5, eaaw4132. https://doi.org/10.1126/sciadv.aaw4132.
Feng, S., Cook, J.M., Anesio, A.M., Benning, L.G., Tranter, M., 2023. Long time series (1984–2020) of albedo variations on the Greenland ice sheet from harmonized Landsat and Sentinel 2 imagery. J. Glaciol. 1–16. https://doi.org/10.1017/jog.2023.11.
Fettweis, X., Box, J.E., Agosta, C., Amory, C., Kittel, C., Lang, C., van As, D., Machguth, H., Gallée, H., 2017. Reconstructions of the 1900–2015 Greenland ice sheet surface mass balance using the regional climate MAR model. The Cryosphere 11, 1015–1033. https://doi.org/10.5194/tc-11-1015-2017.
Fettweis, X., Hofer, S., Séférian, R., Amory, C., Delhasse, A., Doutreloup, S., Kittel, C., Lang, C., Van Bever, J., Veillon, F., Irvine, P., 2021. Brief communication: reduction in the future Greenland ice sheet surface melt with the help of solar geoengineering. The Cryosphere 15, 3013–3019. https://doi.org/10.5194/tc-15-3013-2021.
Fitzpatrick, A.A.W., Hubbard, A.L., Box, J.E., Quincey, D.J., Van As, D., Mikkelsen, A.P. B., Doyle, S.H., Dow, C.F., Hasholt, B., Jones, G.A., 2014. A decade (2002–2012) of supraglacial lake volume estimates across Russell Glacier, West Greenland. The Cryosphere 8, 107–121. https://doi.org/10.5194/tc-8-107-2014.
Fricker, H.A., Arndt, P., Brunt, K.M., Datta, R.T., Fair, Z., Jasinski, M.F., Kingslake, J., Magruder, L.A., Moussavi, M., Pope, A., Spergel, J.J., Stoll, J.D., Wouters, B., 2021. ICESat-2 meltwater depth estimates: application to surface melt on Amery Ice Shelf, East Antarctica. Geophys. Res. Lett. 48, e2020GL090550. https://doi.org/10.1029/2020GL090550.
Goelles, T., Bøggild, C.E., 2017. Albedo reduction of ice caused by dust and black carbon accumulation: a model applied to the K-transect, West Greenland. J. Glaciol. 63, 1063–1076. https://doi.org/10.1017/jog.2017.74.
Goward, S.N., Masek, J.G., Williams, D.L., Irons, J.R., Thompson, R.J., 2001. The Landsat 7 mission: Terrestrial research and applications for the 21st century. Remote Sens. Environ., Landsat 7 78, 3–12. https://doi.org/10.1016/S0034-4257(01)00262-0.
Hanna, E., Cappelen, J., Fettweis, X., Mernild, S.H., Mote, T.L., Mottram, R., Steffen, K., Ballinger, T.J., Hall, R.J., 2021. Greenland surface air temperature changes from 1981 to 2019 and implications for ice-sheet melt and mass-balance change. Int. J. Climatol. 41, E1336–E1352. https://doi.org/10.1002/joc.6771.
How P., Abermann J., Ahlstrøm A.P., Andersen S.B., Box J.E., Citterio M., Colgan W.T., R. S F., Karlsson N.B., Jakobsen J., Langley K., Larsen S.H., Lund M.C., Mankoff K.D., Pedersen A.Ø., Rutishauser A., Shield C.L., Solgaard A.M., van As D., Vandecrux B., Wright P.J., 2022. PROMICE and GC-Net automated weather station data in Greenland. https://doi.org/10.22008/FK2/IW73UU.
Hu, J., Huang, H., Chi, Z., Cheng, X., Wei, Z., Chen, P., Xu, X., Qi, S., Xu, Y., Zheng, Y., 2022. Distribution and evolution of supraglacial lakes in Greenland during the 2016–2018 melt seasons. Remote Sens. 14, 55. https://doi.org/10.3390/rs14010055.
Huai, B., van den Broeke, M.R., Reijmer, C.H., Cappellen, J., 2021. Quantifying rainfall in Greenland: a combined observational and modeling approach. J. Appl. Meteorol. Climatol. 60, 1171–1188. https://doi.org/10.1175/JAMC-D-20-0284.1.
Ahmadianfar, I., Samadi-Koucheksaraee, A., Razavi, S., 2023. Design of optimal operating rule curves for hydropower multi-reservoir systems by an influential optimization method. Renew. Energy 211, 508–521. https://doi.org/10.1016/j.renene.2023.04.113.
Jiang, D., Li, X., Zhang, K., Marinsek, S., Hong, W., Wu, Y., 2022. Automatic supraglacial lake extraction in Greenland using Sentinel-1 SAR images and attention-based U-Net. Remote Sens. 14, 4998. https://doi.org/10.3390/rs14194998.
Johansson, A.M., Jansson, P., Brown, I.A., 2013. Spatial and temporal variations in lakes on the Greenland Ice Sheet. J. Hydrol. 476, 314–320. https://doi.org/10.1016/j.jhydrol.2012.10.045.
Kordani, M., Nikoo, M.R., Fooladi, M., Ahmadianfar, I., Nazari, R., Gandomi, A.H., 2024. Improving long-term flood forecasting accuracy using ensemble deep learning Models and an attention mechanism. J. Hydrol. Eng. 29, 04024042. https://doi.org/10.1061/JHYEFF.HEENG-6262.
Law, R., Arnold, N., Benedek, C., Tedesco, M., Banwell, A., Willis, I., 2020. Over-winter persistence of supraglacial lakes on the Greenland Ice Sheet: results and insights from a new model. J. Glaciol. 66, 362–372. https://doi.org/10.1017/jog.2020.7.
Leeson, A.A., Eastoe, E., Fettweis, X., 2018. Extreme temperature events on Greenland in observations and the MAR regional climate model. The Cryosphere 12, 1091–1102. https://doi.org/10.5194/tc-12-1091-2018.
Leeson, A.A., Shepherd, A., Briggs, K., Howat, I., Fettweis, X., Morlighem, M., Rignot, E., 2015. Supraglacial lakes on the Greenland ice sheet advance inland under warming climate. Nat. Clim. Change. 5, 51–55. https://doi.org/10.1038/nclimate2463.
Leeson, A.A., Shepherd, A., Palmer, S., Sundal, A., Fettweis, X., 2012. Simulating the growth of supraglacial lakes at the western margin of the Greenland ice sheet. The Cryosphere 6, 1077–1086. https://doi.org/10.5194/tc-6-1077-2012.
Legleiter, C.J., Tedesco, M., Smith, L.C., Behar, A.E., Overstreet, B.T., 2014. Mapping the bathymetry of supraglacial lakes and streams on the Greenland ice sheet using field measurements and high-resolution satellite images. The Cryosphere 8, 215–228. https://doi.org/10.5194/tc-8-215-2014.
Li, Z., Erb, A., Sun, Q., Liu, Y., Shuai, Y., Wang, Z., Boucher, P., Schaaf, C., 2018. Preliminary assessment of 20-m surface albedo retrievals from sentinel-2A surface reflectance and MODIS/VIIRS surface anisotropy measures. Remote Sens. Environ. 217, 352–365. https://doi.org/10.1016/j.rse.2018.08.025.
Liang, S., 2000. Narrowband to broadband conversions of land surface albedo I Algorithms. Remote Sens. Environ. 76, 213–238.
Linden, P.F., 2000. Convection in the environment. In: Perspectives in Fluid Dynamics. Cambridge University Press, Cambridge, pp. 287–343.
Lu, Y., Yang, K., Lu, X., Li, Y., Gao, S., Mao, W., Li, M., 2021. Response of supraglacial rivers and lakes to ice flow and surface melt on the northeast Greenland ice sheet during the 2017 melt season. J. Hydrol. 602, 126750. https://doi.org/10.1016/j.jhydrol.2021.126750.
Lüthje, M., Pedersen, L.T., Reeh, N., Greuell, W., 2006. Modelling the evolution of supraglacial lakes on the West Greenland ice-sheet margin. J. Glaciol. 52, 608–618. https://doi.org/10.3189/172756506781828386.
Lutz, K., Bever, L., Sommer, C., Seehaus, T., Humbert, A., Scheinert, M., Braun, M., 2024. Assessing supraglacial lake depth using ICESat-2, Sentinel-2, TanDEM-X, and in situ sonar measurements over Northeast and Southwest Greenland. The Cryosphere 18, 5431–5449. https://doi.org/10.5194/tc-18-5431-2024.
Maier, N., Andersen, J.K., Mouginot, J., Gimbert, F., Gagliardini, O., 2023. Wintertime supraglacial lake drainage cascade triggers large-scale ice flow response in Greenland. Geophys. Res. Lett. 50, e2022GL102251. https://doi.org/10.1029/2022GL102251.
Malambo, L., Popescu, S., 2020. PhotonLabeler: an inter-disciplinary platform for visual interpretation and labeling of ICESat-2 geolocated photon data. Remote Sens. 12, 3168. https://doi.org/10.3390/rs12193168.
Man, M., Yang, K., Chen, D., Zhu, Y., Wang, Y., 2025. Estimating supraglacial lake depth in Greenland: a comparison study of empirical formula, radiative transfer and depression topography methods. J. Glaciol. 71, e41.
Markus, T., Neumann, T., Martino, A., Abdalati, W., Brunt, K., Csatho, B., Farrell, S., Fricker, H., Gardner, A., Harding, D., Jasinski, M., Kwok, R., Magruder, L., Lubin, D., Luthcke, S., Morison, J., Nelson, R., Neuenschwander, A., Palm, S., Popescu, S., Shum, C., Schutz, B.E., Smith, B., Yang, Y., Zwally, J., 2017. The Ice, Cloud, and land Elevation Satellite-2 (ICESat-2): Science requirements, concept, and implementation. Remote Sens. Environ. 190, 260–273. https://doi.org/10.1016/j.rse.2016.12.029.
Melling, L., Leeson, A., McMillan, M., Maddalena, J., Bowling, J., Glen, E., Sandberg Sørensen, L., Winstrup, M., Lørup Arildsen, R., 2024. Evaluation of satellite methods

for estimating supraglacial lake depth in southwest Greenland. The Cryosphere 18, 543–558. https://doi.org/10.5194/tc-18-543-2024.
Morassutti, M.F., LeDrew, E.F., 1996. Albedo and depth of melt ponds on sea-ice. Int. J. Climatol. 16, 817–838.
Neumann, T., Anita Brenner, David Hancock, John Robbins, Aimée Gibbons, Jeffrey Lee, Kaitlin Harbeck, Jack Saba, Scott Luthcke, Tim Rebold, 2022. Ice, Cloud, and Land Elevation Satellite (ICESat-2) Project Algorithm Theoretical Basis Document (ATBD) for Global Geolocated Photons ATL03, Version 6. ICESat-2 Project. https://doi.org/10.5067/GA5KCLJT7LOT.
Neumann, T.A., Martino, A.J., Markus, T., Bae, S., Bock, M.R., Brenner, A.C., Brunt, K.M., Cavanaugh, J., Fernandes, S.T., Hancock, D.W., Harbeck, K., Lee, J., Kurtz, N.T., Luers, P.J., Luthcke, S.B., Magruder, L., Pennington, T.A., Ramos-Izquierdo, L., Rebold, T., Skoog, J., Thomas, T.C., 2019. The Ice, Cloud, and land elevation satellite – 2 mission: a global geolocated photon product derived from the advanced topographic laser altimeter system. Remote Sens. Environ. 233, 111325. https://doi.org/10.1016/j.rse.2019.111325.
Noël, B., van de Berg, W.J., Machguth, H., Lhermitte, S., Howat, I., Fettweis, X., van den Broeke, M.R., 2016. A daily, 1 km resolution data set of downscaled Greenland ice sheet surface mass balance (1958–2015). The Cryosphere 10, 2361–2377. https://doi.org/10.5194/tc-10-2361-2016.
Noël, B., van de Berg, W.J., van Meijgaard, E., Kuipers Munneke, P., van de Wal, R.S.W., van den Broeke, M.R., 2015. Evaluation of the updated regional climate model RACMO2.3: summer snowfall impact on the Greenland Ice Sheet. The Cryosphere 9, 1831–1844. https://doi.org/10.5194/tc-9-1831-2015.
Onuma, Y., Takeuchi, N., Tanaka, S., Nagatsuka, N., Niwano, M., Aoki, T., 2018. Observations and modelling of algal growth on a snowpack in north-western Greenland. The Cryosphere 12, 2147–2158. https://doi.org/10.5194/tc-12-2147-2018.
Parrish, C.E., Magruder, L.A., Neuenschwander, A.L., Forfinski-Sarkozi, N., Alonzo, M., Jasinski, M., 2019. Validation of ICESat-2 ATLAS bathymetry and analysis of ATLAS's Bathymetric mapping performance. Remote Sens. 11, 1634. https://doi.org/10.3390/rs11141634.
Pegau, W.S., Gray, D., Zaneveld, J.R.V., 1997. Absorption and attenuation of visible and near-infrared light in water: dependence on temperature and salinity. Appl. Opt. 36, 6035–6046.
Pope, A., Scambos, T.A., Moussavi, M., Tedesco, M., Willis, M., Shean, D., Grigsby, S., 2016. Estimating supraglacial lake depth in West Greenland using Landsat 8 and comparison with other multispectral methods. The Cryosphere 10, 15–27. https://doi.org/10.5194/tc-10-15-2016.
Qu, Y., Liang, S., Liu, Q., He, T., Liu, S., Li, X., 2015. Mapping surface broadband albedo from satellite observations: a review of literatures on algorithms and products. Remote Sens. 7, 990–1020. https://doi.org/10.3390/rs70100990.
Ran, J., Ditmar, P., van den Broeke, M.R., Liu, L., Klees, R., Khan, S.A., Moon, T., Li, J., Bevis, M., Zhong, M., Fettweis, X., Liu, J., Noël, B., Shum, C.K., Chen, J., Jiang, L., van Dam, T., 2024. Vertical bedrock shifts reveal summer water storage in Greenland ice sheet. Nature 635, 108–113. https://doi.org/10.1038/s41586-024-08096-3.
Samadi-koucheksaraee, A., Ahmadianfar, I., Bozorg-Haddad, O., Asghari-pari, S.A., 2019. Gradient evolution optimization algorithm to optimize reservoir operation systems. Water Resour. Manage. 33, 603–625. https://doi.org/10.1007/s11269-018-2122-2.
Samadi-Koucheksaraee, A., Chu, X., 2024. Development of a novel modeling framework based on weighted kernel extreme learning machine and ridge regression for streamflow forecasting. Sci. Rep. 14, 30910. https://doi.org/10.1038/s41598-024-81779-z.
Smith, B.E., Medley, B., Fettweis, X., Sutterley, T., Alexander, P., Porter, D., Tedesco, M., 2023. Evaluating Greenland surface-mass-balance and firn-densification data using ICESat-2 altimetry. The Cryosphere 17, 789–808. https://doi.org/10.5194/tc-17-789-2023.
Smith, R.C., Baker, K.S., 1981. Optical properties of the clearest natural waters (200–800 nm). Appl. Opt. 20, 177. https://doi.org/10.1364/AO.20.000177.
Steffen K., Vandecrux B., Houtz D., Abdalati W., Bayou N., Box J.E., Colgan W.T., Espona Pernas L., Griessinger N., Haas-Artho D., Heilig A., Hubert A., Iosifescu Enescu I., Johnson-Amin N., Karlsson N.B., Kurup Buchholz R., McGrath D., Cullen N.J., Naderpour R., Molotch N.P., Pedersen A.Ø., Perren B., Philipps T., Plattner G.-K., Proksch M., Revheim M.K., Særrelse M., Schneebli M., Sampson K., Starkweather S., Steffen S., Stroeve J., Watler B., Winton Ø.A., Zwally J., Ahlstrøm A., 2022. GC-Net Level 1 historical automated weather station data. https://doi.org/10.22008/FK2/VVXGUT.
Stibal, M., Box, J.E., Cameron, K.A., Langen, P.L., Yallop, M.L., Mottram, R.H., Khan, A. L., Molotch, N.P., Chrismas, N.A.M., Calì Quaglia, F., Remias, D., Smeets, C.J.P.P., van den Broeke, M.R., Ryan, J.C., Hubbard, A., Tranter, M., van As, D., Ahlstrøm, A. P., 2017. Algae drive enhanced darkening of bare ice on the Greenland Ice Sheet. Geophys. Res. Lett. 44, 11463–11471. https://doi.org/10.1002/2017GL075958.
Tedesco, M., Lüthje, M., Steffen, K., Steiner, N., Fettweis, X., Willis, I., Bayou, N., Banwell, A., 2012. Measurement and modeling of ablation of the bottom of supraglacial lakes in western Greenland. Geophys. Res. Lett. 39. https://doi.org/10.1029/2011GL049882.
Tedesco, M., Steiner, N., 2011. In-situ multispectral and bathymetric measurements over a supraglacial lake in western Greenland using a remotely controlled watercraft. The Cryosphere 5, 445–452. https://doi.org/10.5194/tc-5-445-2011.
Tedstone, A.J., Cook, J.M., Williamson, C.J., Hofer, S., McCutcheon, J., Irvine-Fynn, T., Gribbin, T., Tranter, M., 2020. Algal growth and weathering crust state drive variability in western Greenland Ice Sheet ice albedo. The Cryosphere 14, 521–538. https://doi.org/10.5194/tc-14-521-2020.
Timmermans, G., Fettweis, X., 2024. Impact of supraglacial lakes on the Greenland Ice Sheet Surface Mass Balance into the regional climate model MAR (No. EGU24-18932). Presented at the EGU24, Copernicus Meetings. https://doi.org/10.5194/egusphere-egu24-18932.
van den Broeke, M., Box, J., Fettweis, X., Hanna, E., Noël, B., Tedesco, M., van As, D., van de Berg, W.J., van Kampenhout, L., 2017. Greenland ice sheet surface mass loss: recent developments in observation and modeling. Curr. Clim. Change Rep. 3, 345–356. https://doi.org/10.1007/s40641-017-0084-8.
van Meijgaard, E., van Ulft, L.H., van de Berg, W.J., Bosveld, F.C., van den Hurk, B.J.J. M., Lenderink, G., Siebesma, A.P., 2008. The KNMI regional atmospheric climate model RACMO, version 2. The Netherlands: KNMI, De Bilt.
van Tiggelen, M., Smeets, P.C.J.P., Reijmer, C.H., Wouters, B., Steiner, J.F., Nieuwstraten, E.J., Immerzeel, W.W., van den Broeke, M.R., 2021. Mapping the aerodynamic roughness of the Greenland Ice Sheet surface using ICESat-2: evaluation over the K-transect. The Cryosphere 15, 2601–2621. https://doi.org/10.5194/tc-15-2601-2021.
Vandecrux, B., Box, J.E., Ahlstrøm, A.P., Andersen, S.B., Bayou, N., Colgan, W.T., Cullen, N.J., Fausto, R.S., Haas-Artho, D., Heilig, A., Houtz, D.A., How, P., Iosifescu Enescu, I., Karlsson, N.B., Kurup Buchholz, R., Mankoff, K.D., McGrath, D., Molotch, N.P., Perren, B., Revheim, M.K., Rutishauser, A., Sampson, K., Schneebeli, M., Starkweather, S., Steffen, S., Weber, J., Wright, P.J., Zwally, H.J., Steffen, K., 2023. The historical Greenland climate Network (GC-Net) curated and augmented level-1 dataset. Earth Syst. Sci. Data. 15, 5467–5489. https://doi.org/10.5194/essd-15-5467-2023.
Williamson, A.G., Banwell, A.F., Willis, I.C., Arnold, N.S., 2018. Dual-satellite (Sentinel-2 and Landsat 8) remote sensing of supraglacial lakes in Greenland. The Cryosphere 12, 3045–3065. https://doi.org/10.5194/tc-12-3045-2018.
Williamson, C.J., Cook, J., Tedstone, A., Yallop, M., McCutcheon, J., Poniecka, E., Campbell, D., Irvine-Fynn, T., McQuaid, J., Tranter, M., Perkins, R., Anesio, A., 2020. Algal photophysiology drives darkening and melt of the Greenland Ice Sheet. Proc. Natl. Acad. Sci. 117, 5694–5705. https://doi.org/10.1073/pnas.1918412117.
Xiao, W., Hui, F., Cheng, X., Liang, Q., 2023. An automated algorithm to retrieve the location and depth of supraglacial lakes from ICESat-2 ATL03 data. Remote Sens. Environ. 298, 113730. https://doi.org/10.1016/j.rse.2023.113730.
Yang, K., Smith, L.C., 2013. Supraglacial streams on the Greenland Ice Sheet delineated from combined spectral–shape information in high-resolution satellite imagery. IEEE Geosci. Remote Sensing Lett. 10, 801–805. https://doi.org/10.1109/LGRS.2012.2224316.
Yang, K., Smith, L.C., Fettweis, X., Gleason, C.J., Lu, Y., Li, M., 2019. Surface meltwater runoff on the Greenland ice sheet estimated from remotely sensed supraglacial lake infilling rate. Remote Sens. Environ. 234, 111459. https://doi.org/10.1016/j.rse.2019.111459.
Yang, K., Smith, L.C., Karlstrom, L., Cooper, M.G., Tedesco, M., van As, D., Cheng, X., Chen, Z., Li, M., 2018. A new surface meltwater routing model for use on the Greenland Ice Sheet surface. The Cryosphere 12, 3791–3811. https://doi.org/10.5194/tc-12-3791-2018.
Zhang, Q., Huai, B., van den Broeke, M.R., Cappelen, J., Ding, M., Wang, Y., Sun, W., 2022. Temporal and spatial variability in contemporary Greenland warming (1958–2020). J. Climate. 35, 2755–2767. https://doi.org/10.1175/JCLI-D-21-0313.1.
Zhang, W., Yang, K., Smith, L.C., Wang, Y., van As, D., Noël, B., Lu, Y., Liu, J., 2023. Pan-Greenland mapping of supraglacial rivers, lakes, and water-filled crevasses in a cool summer (2018) and a warm summer (2019). Remote Sens. Environ. 297, 113781. https://doi.org/10.1016/j.rse.2023.113781.
Zheng, L., Li, L., Chen, Z., He, Y., Mo, L., Chen, D., Hu, Q., Wang, L., Liang, Q., Cheng, X., 2023. Multi-sensor imaging of winter buried lakes in the Greenland Ice Sheet. Remote Sens. Environ. 295, 113688. https://doi.org/10.1016/j.rse.2023.113688.
Zhou, Q., Liang, Q., Xiao, W., Li, T., Zheng, L., Cheng, X., 2025. Supraglacial lake depth retrieval from ICESat-2 and multispectral imagery datasets. J. Remote Sens. 5, 0416. https://doi.org/10.34133/remotesensing.0416.